Small structural changes account for the high thermostability of 1[4Fe–4S] ferredoxin from the hyperthermophilic bacterium *Thermotoga maritima*

Sandra Macedo-Ribeiro[1]*, Beatrice Darimont[2†], Reinhard Sterner[2] and Robert Huber[1]

Background: The characterization of the structural features that account for the high thermostability of some proteins is of great scientific and biotechnological interest. Proteins from hyperthermophilic organisms with optimum growth temperatures of 80° C and higher generally show high intrinsic stabilities. The comparison of high resolution X-ray structures of these proteins with their counterparts from mesophilic organisms has therefore helped to identify potentially stabilizing forces in a number of cases. Small monomeric proteins which comprise only a single domain, such as ferredoxins, are especially suitable for such comparisons since the search for determinants of protein stability is considerably simplified.

Results: The 1.75 Å crystal structure of the extremely thermostable 1[4Fe–4S] ferredoxin from *Thermotoga maritima* (Fd_{Tm}) was determined and compared with other monocluster-containing ferredoxins with different degrees of thermostability.

Conclusions: A comparison of the three-dimensional structure of Fd_{Tm} with that of ferredoxins from mesophilic organisms suggests that the very high thermostability of Fd_{Tm} is unexpectedly achieved without large changes of the overall protein structure. Instead, an increased number of potentially stabilizing features is observed in Fd_{Tm}, compared with mesophilic ferredoxins. These include stabilization of α helices, replacement of residues in strained conformation by glycines, strong docking of the N-terminal methionine and an overall increase in the number of hydrogen bonds. Most of these features stabilize several secondary structure elements and improve the overall rigidity of the polypeptide backbone. The decreased flexibility will certainly play a relevant role in shielding the iron–sulfur cluster against physiologically high temperatures and further improve the functional integrity of Fd_{Tm}.

Addresses: [1]Max-Planck Institut für Biochemie, D-82152 Martinsried, Germany and [2]Abteilung Biophysikalische Chemie, Biozentrum, Universität Basel, CH-4056 Basel, Switzerland.

[†]Present address: Department of Cellular and Molecular Pharmacology, University of California, San Francisco, CA 94143-0450, USA.

*Corresponding author.
E-mail: ribeiro@biochem.mpg.de

Key words: crystal structure, hydrogen bonds, iron-sulfur protein, thermostability, turns

Received: 19 July 1996
Revisions requested: 19 August 1996
Revisions received: 12 September 1996
Accepted: 17 September 1996

Structure 15 November 1996, 4:1291–1301

Introduction

Iron-sulfur clusters are ubiquitous in electron transfer proteins involved in fundamental biological processes such as photosynthesis, oxidative phosphorylation and nitrogen fixation. Ferredoxins are amongst the most simple iron-sulfur proteins participating in these pathways. Prokaryotic ferredoxins mostly contain either one or two [4Fe–4S] (or [3Fe–4S]) clusters [1]. The polypeptide chain in ferredoxins is involved in the fine-tuning of the cluster activity and in the mediation of its interaction with the redox partners. The ferredoxin from the hyperthermophilic bacterium *Thermotoga maritima* (Fd_{Tm}) is a monomer containing 60 amino acid residues and a single [4Fe–4S] cluster [2,3]. Differential scanning calorimetry studies show that Fd_{Tm} has a transition temperature of 125°C and thus represents one of the most thermostable proteins that have been investigated so far (W Pfeil, U Gesierich, RS, unpublished results). Fd_{Tm} displays a high degree of sequence homology with other ferredoxins from the hyperthermophilic archaea *Thermoccocus litoralis* (Fd_{Tl}) and *Pyrococcus furiosus* (Fd_{Pf}) (75% and 48% sequence identity, respectively). Curiously the sequence similarity to bacterial ferredoxins is not higher than 43%. Of the ferredoxins containing 1[4Fe–4S] or 1[3Fe–4S] clusters (monocluster-type ferredoxins) the X-ray structures of 1[3Fe–4S] Fd_{Dg} [4], 1[4Fe–4S] Fd_{Daf} [5] and 1[4Fe–4S] Fd_{Bt} [6] are known. The secondary structures of the 1[4Fe–4S] Fd_{Tl} [7] and 1[3Fe–4S] Fd_{Pf} [8] have also been determined by ^{1}H NMR and recently a NMR-derived model of 1[4Fe–4S] Fd_{Tm} has been reported [9].

Here we report the crystallization, X-ray structure analysis and model refinement of Fd_{Tm} at 1.75 Å resolution. The structure was determined by Patterson search methods using Fd_{Dg} [4] as a search model. This first high resolution structure of an extremely thermostable ferredoxin allows

detailed comparisons with ferredoxins from mesophilic organisms which exhibit remarkable similarities with Fd_{Tm} in terms of sequence and redox properties. The fine structural differences that may be responsible for the drastically increased thermostability of Fd_{Tm} are discussed.

Results and discussion

Overall topology

Thermotoga maritima ferredoxin (Fd_{Tm}) forms a cylindrical structure of dimensions 25×23×21 Å^3 (Fig. 1a). The overall folding of the protein seems to be influenced by non-peptide interactions to the large metal cluster, as shown by the absence of secondary structure in the apo- form of the Fd_{Tm} [3]. A schematic drawing of the Fd_{Tm} structure is depicted in Figure 1b, highlighting the secondary structure elements. As predicted from the high homology with other monocluster-containing ferredoxins (Fig. 2) Fd_{Tm} shares a common topology with other ferredoxins of known structure, independently of the type ([4Fe–4S] or [3Fe–4S]) of iron-sulfur clusters present [4–6]. This similarity is extended additionally to dicluster-containing ferredoxins [10–13].The largest secondary structure element is α helix H2 (Fig. 1b, Fig. 2) , a three-turn helix including residues Pro42–Ser50, which is common to all ferredoxins lacking a second iron-sulfur cluster [6]. Additionally, there is a second one-turn α-helical segment (helix H1) composed of residues Val15–Leu19 antiparallel to H2, two antiparallel two-stranded β sheets—B1 (residues Lys2–Val5 and Ile56–Glu59) and B2 (residues Phe24–Gly27 and Lys31–Val34)—and five reverse turns (A–E). Turn A is composed of two intercalating turns of type I (Asp6–Ala9 and Ala7–Cys10) and resembles a stretch of 3_{10} helix. The first segment of each turn A (Asp6–Ala9), C (Asp28–Gly30) and E (Cys51–Gly54) is a type I/Asx reverse turn [4,14]. Turn B (Cys20–Val23) can also be classified as a type I turn. The turn containing residues Gln36–Leu41 (turn D) is unusual because it involves no internal main chain hydrogen bonds, but the side chain of Thr39 is hydrogen bonded to the main-chain amide groups of both Asp40 and Leu 41 with very good hydrogen bond geometry (Table 1,2). Turn D is further stabilized by a strong hydrogen bond between the side chains of Gln36 and Thr39 (Table 2). This region, its specific interactions and implications for thermostability will be discussed further on.

In the NMR solution structure for Fd_{Tm} the region Gly27–Gln36 forms a flexible loop, but β sheet B2 could not be safely determined [9]. In fact, this region presents very high B values in the present X-ray structure similar to Fd_{Dg} [4] and in Fd_{Daf} [5].

A disulfide bridge is formed between Cys20 and Cys43, whose side chains form a right-handed spiral. This disulfide bridge is found in some monocluster-type ferredoxins such as Fd_{Dg} but is absent in Fd_{Bt} and in Fd_{Daf}, which do not contain cysteine residues at the corresponding positions (Fig. 2). The presence of this disulfide bridge was previously proposed on the basis of chemical analysis [3] and confirmed in the Fd_{Tm} NMR-derived model [9]. Further experiments will show whether this disulfide is involved in the redox cycle of Fd_{Tm}, as is the case for Fd_{Dg} and Fd_{Pf} [15,16].

Figure 1

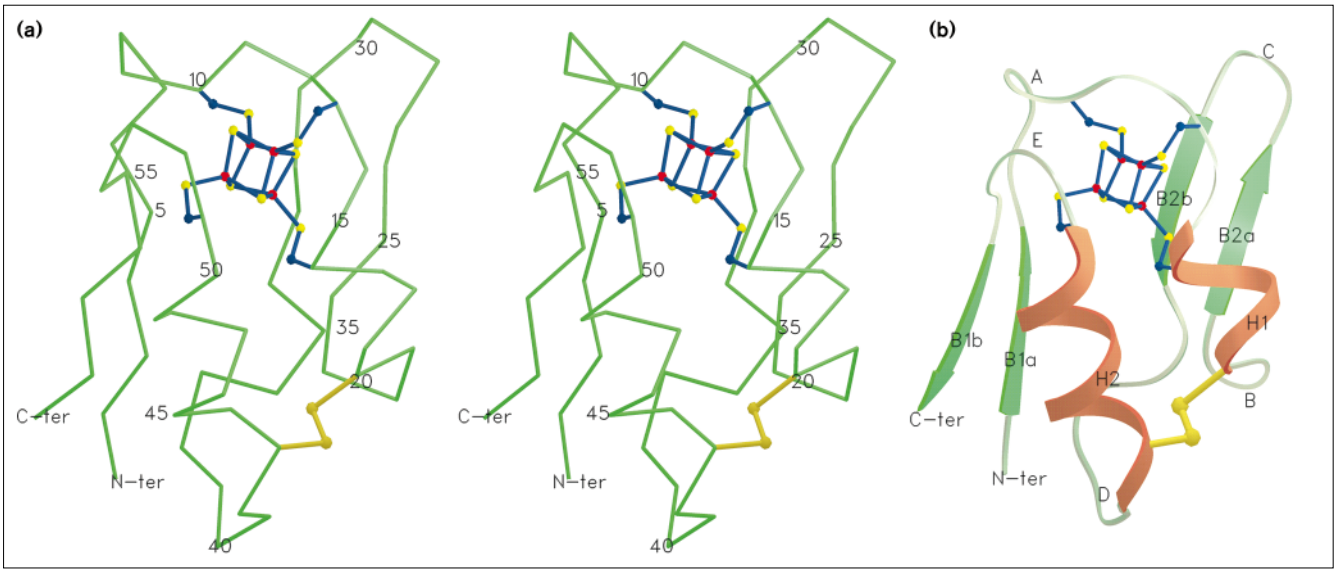

Representation of the Fd_{Tm} structure. (a) Stereo view of the Cα backbone; each fifth residue is labeled. (b) Schematic representation of the Fd_{Tm} structure. B1, B2: β sheets; H1, H2: α helices; A–E: turns. Iron atoms of the cluster are shown in red and all sulfur atoms are shown in yellow.

Figure 2

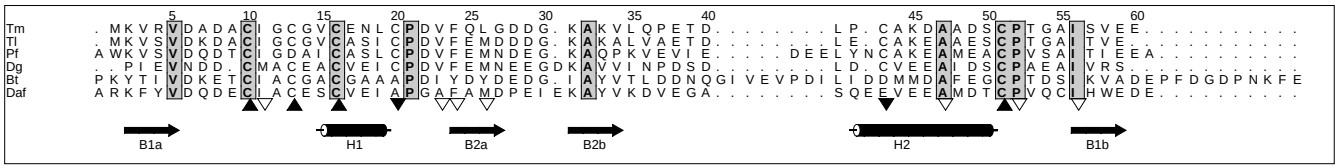

Structure-based amino acid sequence alignment of monocluster-type ferredoxins. Numbers refer to the Fd_{Tm} sequence. Residues that are conserved among listed ferredoxins are shaded. Symbols: ▲, cluster-binding residues; ▼, cysteines involved in the disulfide bridge in Fd_{Tm}; ▽, highly conserved hydrophobic residues which shield the cluster from direct solvent contact. The secondary structure elements of Fd_{Tm} are very similar to those of all shown ferredoxins and marked as in Figure 1: Tm, *Thermotoga maritima* [3]; Tl, *Thermococcus litoralis* [51]; Pf, *Pyrococcus furiosus* [51]; Dg, *Desulfovibrio gigas* [4,52]; Bt, *Bacillus thermoproteolyticus* [5,53]; Daf, *Desulfovibrio africanus* [5,54].

There is a predominance of negatively charged side-chains although their distribution is rather uniform over the surface of the protein and there is no clustering of negative charges in any particular region. The side chains of Asp6, Asp29 and Glu38 are involved in interactions with main chain atoms. The positively charged side chains of Lys2, Lys33 and Lys45 are exposed, but Lys31 and Arg4 interact with main-chain atoms through hydrogen bonds (see Table 2).

Geometry and environment of the 1[4Fe–4S] cluster

The 1[4Fe–4S] cluster is covalently attached to the protein by Fe–Sγ bonds at cysteine residues 10, 13, 16 and 51. A representative electron density for the cluster binding region is displayed in Figure 3. This cluster is located at the upper part of the molecule, according to the standard orientation as displayed in Figure 1b, and very close to its surface. It is protected from direct solvent contact by the cluster binding segment Cys10 to Cys16 and by the hydrophobic core which includes the side chains from residues Ile11, Val23, Phe24, Leu26, Ala32, Pro52 and Ile56 (Fig. 4). Three of the inorganic sulfur atoms in the cluster and the four cluster-binding Sγ atoms from the protein moiety are involved in an asymmetrical network of NH...S hydrogen bonds with main-chain nitrogen atoms from residues surrounding the cluster (Table 3). The [4Fe–4S] cluster in Fd_{Tm} exhibits Fe–S bond distances and bond angles for the bridging and terminal sulfur atoms which are in good agreement with those found in Fd_{Daf} [5], Fd_{Bt} [6] and in other [4Fe–4S] ferredoxins of known structure [10–13]. Differences in the exact values for these distances and angles determined by crystallographic studies are largely dependent on the accuracies of the models. It should be noted that the differences observed for the [4Fe–4S] cluster in distinct ferredoxins are comparable to differences observed between clusters from ferredoxin molecules present in the same asymmetric unit [5], or between each [4Fe–4S] cluster in dicluster-containing ferredoxins [10,13].

The cluster environment has been suggested to play a role in the stability and redox potential of ferredoxins and other iron-sulfur proteins. Features such as the number and strength of NH...S hydrogen bonds, the side chains in the vicinity of the cluster and the degree of solvent exposure determine the main characteristics of this environment, although the extent of contribution from each of these factors to the redox potential of iron-sulfur proteins is still a matter of debate [17,18]. 1[4Fe–4S] Fd_{Tm}, 1[4Fe–4S] Fd_{Daf} and 1[3Fe–4S] Fd_{Dg} have redox potentials of –388 mV [19], –385 mV [20] and –130 mV [21], respectively. Clearly the high redox potential for Fd_{Dg} might be explained by the absence of one iron in the cluster since the 1[4Fe–4S] form of this ferredoxin has a

Figure 3

Representative electron density of Fd_{Tm}. The region around the iron-sulfur cluster is shown. The final ($2F_o–F_c$) map is contoured at 1.5σ level. The cluster and the cluster-complexing residues are shown in yellow.

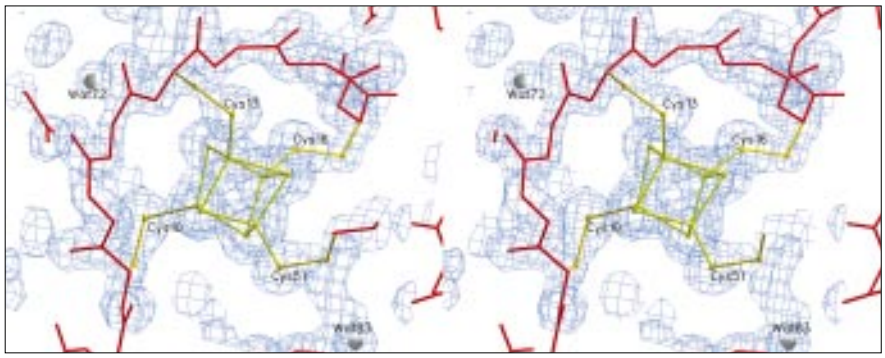

Table 1

Possible hydrogen bonds in Fd_{Tm}: hydrogen bonds involving main-chain protein atoms.

Donor (D)		Acceptor (A)		Distance D…A (Å)
Met1	N	Thr39	O	2.77
Lys2	N	Glu59	O	2.75
Val3	N	Pro37	O	2.76
Arg4	N	Ser57	O	3.00
Asp6	N	Ala55	O	2.80
Ala9	N	Asp6	O	3.02
Cys10	N	Asp6	O	3.14
Glu17	N	Gly14	O	3.14
Asn18	N	Gly14	O	3.17
Leu19	N	Val15	O	3.03
Cys20	N	Cys16	O	2.80
Val23	N	Cys20	O	2.91
Phe24	N	Cys20	O	2.93
Gln25	N	Lys33	O	3.03
Gly27	N	Lys31	O	2.78
Gly30	N	Gly27	O	3.12
Lys33	N	Gln25	O	2.72
Leu35	N	Val23	O	2.77
Thr39	N	Met1	O	2.92
Ala44	N	Leu41	O	2.99
Lys45	N	Pro42	O	3.14
Ala47	N	Cys43	O	2.88
Ala48	N	Ala44	O	3.10
Asp49	N	Lys45	O	3.14
Ser50	N	Asp46	O	2.99
Cys51	N	Ala47	O	2.98
Gly54	N	Cys51	O	3.47
Ser57	N	Arg4	O	2.99
Glu59	N	Lys2	O	2.94

redox potential of –455 mV [21]. Fd_{Bt} is expected to have a redox potential of –280 mV, close to the value determined for *Bacillus stearothermophilus* ferredoxin [18]. The number and distribution of amide hydrogen bonds to the cluster is conserved in Fd_{Tm} (Table 3), Fd_{Daf} [5], and Fd_{Bt} [6]. Neither are differences found in the coordination of the iron-sulfur cluster nor in the disposition of the hydrophobic residues in its proximity (Fig. 2, Fig. 4). The higher redox potential in Fd_{Bt} can be partially explained by the presence of bulkier nonpolar groups (Fig. 2) in the vicinity of the cluster which limit solvent accessibility and increase the hydrophobicity of the cluster environment.

Structural comparison between monocluster-type ferredoxins: insights into thermal stability

The X-ray structures of monocluster-type ferredoxins from two mesophiles (Fd_{Dg} and Fd_{Daf}) and a moderate thermophile (Fd_{Bt}) are presently known [4–6] and the secondary structures for three thermophilic ferredoxins have been determined by NMR studies [7,8,22]. As predicted from the high sequence similarity (Fig. 2) and the NMR-derived model of Fd_{Tm} [9], the crystal structures of Fd_{Tm}, Fd_{Dg} and Fd_{Daf} share a similar folding pattern (Fig. 5). The same is valid for the Fd_{Bt}, which has some insertions and a large C-terminal extension in comparison with the other monocluster-type ferredoxins [6]. The only regions that differ notably are turn A, which is shorter by one residue in Fd_{Dg} when compared with all other monocluster-type ferredoxins, and turn C, which is tighter in Fd_{Tm} and in Fd_{Bt}. Fd_{Daf} diverges from Fd_{Tm} mostly in the segment connecting the C terminus of β sheet B2 and the N terminus of α helix H2. Furthermore the surface located N- and C-terminal regions show relatively large deviations in all structures compared in Figure 5. A detailed analysis of all monocluster-type ferredoxins and a comparison with the present Fd_{Tm} model highlight structural differences which can be associated with differences in thermostability. In the following sections it is assumed that Fd_{Tm} is more thermostable than Fd_{Dg} and Fd_{Daf}. Although no studies on the thermostabilities of Fd_{Dg} or Fd_{Daf} have been reported, this assumption seems justified by the extremely high transition temperature of Fd_{Tm} (125° C; W Pfeil, U Gesierich, RS, unpublished results) and by the observation that ferredoxins from thermophiles are generally more heat stable than ferredoxins from mesophiles [23,24]. In this context, a correlation would be expected between the growth temperatures of Pf (100° C),

Table 2

Possible hydrogen bonds in Fd_{Tm}: hydrogen bonds involving side-chain atoms.

Donor (D)		Acceptor (A)		Distance (Å)	Angle D-H…A (°)
Met1	N	Glu38	Oε2	2.86	153.3
Arg4	Nη1	Val13	O	2.94	160.0
Arg4	Nη1	Pro37	O	3.15	124.3
Asp8	N	Asp6	Oδ1	2.98	137.5
Ala9	N	Asp6	Oδ1	3.02	140.9
Leu26	N	Glu17	Oε1	2.86	177.7
Lys31	N	Asp29	Oδ1	3.27	133.3
Lys31	Nζ	Ala7	O	2.75	167.5
Lys31	Nζ	Cys10	O	3.09	122.8
Gln36	Nε2	Asp22	O	3.15	109.2
Thr39	Oγ1	Gln36	Oε1	3.09	167.7
Asp40	N	Thr39	Oγ1	2.87	109.8
Leu41	N	Thr39	Oγ1	3.20	174.0
Asp46	N	Ser50	Oγ1	3.06	145.2
Thr53	Sγ	Ala9	O	2.57	143.6

Table 3

NH...S interactions in Fd_{Tm}.

Donor (D)		Acceptor (A)		Distance D...A (Å)	Angle (D-H…A)(°)
Ile11	N	F4S60	S2	3.30	165.7
Gly14	N	F4S60	S1	3.26	151.5
Cys16	N	F4S60	S4	3.56	133.6
Gly12	N	Cys10	Sγ	3.36	114.0
Ala32	N	Cys10	Sγ	3.44	154.8
Val15	N	Cys13	Sγ	3.50	171.9
Glu17	N	Cys16	Sγ	3.38	113.7
Thr53	N	Cys51	Sγ	3.71	162.1
Ala55	N	Cys51	Sγ	3.41	150.5

Figure 4

The hydrophobic residues around the cluster are highly conserved among monocluster-type ferredoxins. Stereo view of the cluster environment from Fd_{Tm} (side chains in blue), Fd_{Dg} (side chains in orange), Fd_{Daf} (side chains in green) and Fd_{Bt} (side chains in violet) after least-squares superposition. The disulfide bridge present in Fd_{Tm} and Fd_{Dg} is shown in black; the cluster and the side chains of cysteine residues are in blue; for clarity only the Fd_{Tm} backbone and cluster are shown, and the residues from Fd_{Tm} are numbered.

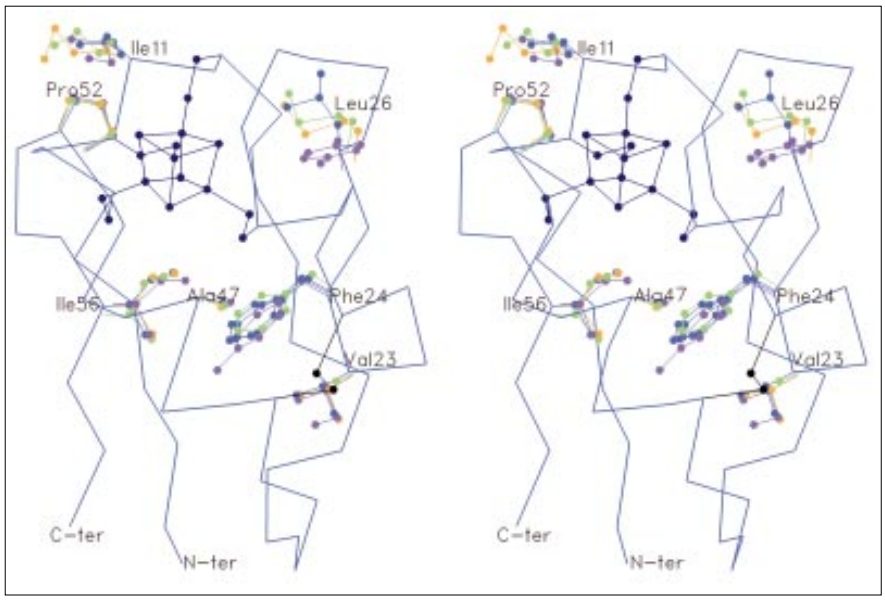

Tl (90° C), Tm (80° C), Bt (60° C), Dg (30–40° C) and Daf (30–40° C) and the relative thermostabilities of the ferredoxins from these organisms.

Stabilization of α helices

Thermal stability has been suggested to be correlated with an increase of the number of alanines in α helices [25–27]. On comparing the sequences of thermophilic ferredoxins with their mesophilic counterparts (Fig. 2), α helix H2, which constitutes the larger secondary structure element in these ferredoxins, shows significant differences in amino acid composition. In fact, the hyperthermophilic ferredoxins Fd_{Tm} and Fd_{Tl} contain three alanine residues in α helix H2, whereas Fd_{Daf}, Fd_{Dg} and Fd_{Bt} have only one. Solution ^{1}H NMR studies show that Fd_{Pf} displays a longer α helix starting at residue Glu43 and running at least until residue Glu54 [8], indicating that this helix contains a minimum of two alanines. In Fd_{Bt}, α helix H1 contains three alanines while in other ferredoxins it contains only one alanine (Fd_{Dg}, Fd_{Pf} and Fd_{Tl}) or no alanines at all (Fd_{Tm} and Fd_{Daf}). Factors such as the extension of α helix H2 (Fd_{Pf}) and replacement of residues with larger side-chains by alanines both in α helix H2 (Fd_{Tm}, Fd_{Tl} and Fd_{Pf}) and in α helix H1 (Fd_{Bt}, Fd_{Tl}, Fd_{Pf} and Fd_{Dg}), when considered independently of other possibly stabilizing factors, seem to contribute to different extents to thermostabilization. Thus, extension of the α helix seems to contribute strongly to thermostabilization, and the contribution provided by the increase in the alanine content of α helices is not strictly linear. Instead, a significant influence arises from

Figure 5

Conserved folding topology within monocluster-type ferredoxins. Least-square superposition of the Cα tracings of Fd_{Tm} (blue), Fd_{Dg} (orange), Fd_{Daf} (green) and Fd_{Bt} (violet). For clarity only the Fd_{Tm} cluster is shown and residue labels refer to Fd_{Tm}.

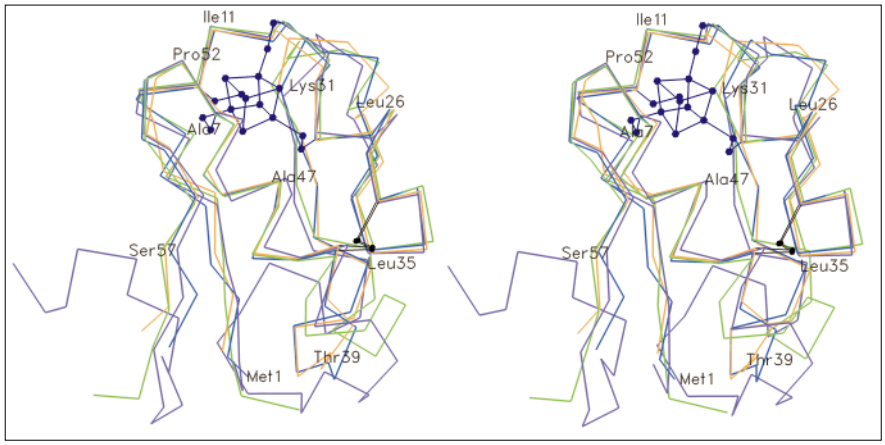

the environment of the additional alanines and from the chemistry of the residues they are replacing.

In addition the carbonyl oxygen atoms at the C-terminal ends of the helices in Fd_{Tm} form hydrogen bonds with a number of water molecules: WAT62 (Glu17 O), WAT85 (Asp49 O and Cys51 O), WAT86 (Asp49 O), and WAT84 (Cys51 O). These interactions are assumed to stabilize α helices [28], and are also found in Fd_{Bt} [6].

Stabilization of the 1[Fe–4S] cluster

The total number of glycines is increased in Fd_{Tm} (and in Fd_{Tl}), compared to other ferredoxins. Most of the additional glycines (Gly12, Gly14, Gly54) are involved (or next to residues involved) in hydrogen bonds to sulfur atoms in the cluster (Table 3). The corresponding residues in Fd_{Dg} (Ala10, Glu12 and Glu53), adopt a left-handed helical conformation which appears to be essential in the formation of the cluster binding cavity and is stabilized by NH...S interactions [4]. In Fd_{Tm} and in Fd_{Tl} the replacement of the residues at these positions by glycines, where no steric hindrance is caused by the left-handed helical conformation, may contribute significantly to the increased stability of the protein. The presence of glycines at some particular positions near the cluster is conserved in hyperthermostable Fd_{Pf} (Gly13) and in moderately thermostable Fd_{Bt} (Gly15). It should be noted at this stage that mesostable ferredoxins Fd_{Dg} and Fd_{Daf} have residues at these positions with side chains that are much larger than the ones from thermostable ferredoxins. This consolidates the hypothesis that this cluster-binding region is stabilized in thermostable ferredoxins through a general release of steric hindrance.

It is known that glycines contribute to the diversity of unfolded conformations and, as a consequence, stabilization by glycine substitution of residues with large side-chains can only be achieved when release of steric hindrance compensates for the normally destabilizing effect associated with the increase of entropy in the unfolded state. Increased thermostability through replacement of residues with positive ϕ dihedral angles by glycines was found in thermostable *Escherichia coli* ribonuclease H1 mutants [29] and in indole-3-glycerol phosphate synthase from the hyperthermophile *Sulfolobus solfataricus* [22].

Further examination of sequence differences between Fd_{Tm} and Fd_{Dg} reveals the loss of two exposed methionines (replaced by Ile11 and Leu26) in the proximity of the cluster in $Fd_{Tm,}$ thus decreasing the content of exposed sulphur-containing side-chains. This could decrease problems associated with the oxidation of side chains at high temperatures [30] in Fd_{Tm}. The extent of the contribution of these substitutions for the particular thermostability of Fd_{Tm} would need further experimental support because they are not conserved in any of the other thermostable ferredoxins. These actually contain methionine in the position corresponding to Leu26 in Fd_{Tm} (Fig. 2). The increase in the number of glycines and the loss of methionines in the cluster binding cavity of Fd_{Tm} could enhance the overall stability of the cluster and thus, help to maintain activity at high temperatures. The cluster ligation could constitute an additional stabilizing interaction. Similarities in the metal sites of ferredoxins seem to indicate that this does not constitute significant strategy for the thermostabilization of Fd_{Tm} relative to mesostable ferredoxins.

Main-chain hydrogen bonds

The N-terminal methionine is fixed to the protein core by two strong hydrogen bonds to the main-chain atoms of Thr39 (Fig. 6, Table 1). Additionally, Val3 N, in β strand B1a, is hydrogen bonded to Pro37 O. In contrast, Fd_{Dg} presents only one hydrogen bond in the same region from Ile2 N to Pro36 O and neither Fd_{Bt} nor Fd_{Daf} show main chain hydrogen bonds to the N terminus [5,6].

NMR investigations suggested that β sheet B1 in Fd_{Pf} and Fd_{Tl} is extended by a third strand, and this feature was considered important for the extreme thermostability of these ferredoxins [7,8]. The segment forming the third strand includes residues Val39–Glu41 in Fd_{Pf} and Ala37–Thr39 in Fd_{Tl}. In Fd_{Tm} the corresponding segment (Pro37–Thr39) does not form a β strand in β sheet B1. However, stabilization could be achieved by fixing Met1 and Val3, which are not involved in the hydrogen bonding pattern of this first β sheet, to the rest of the protein. A similar extension of the hydrogen bond network to the N-terminal residue is observed in the X-ray structure of rubredoxin from *P. furiosus* [31].

Turn C

Turn C is shorter by one residue in Fd_{Tm} and this observation is in good agreement with the data from Fd_{Pf} [8] and Fd_{Tl} [7]. This turn seems to be shorter also in Fd_{Bt} [6]. The data correlate very well with the relative thermostabilities of the different ferredoxins. Shortening of surface located turns, which may act as weak points upon thermal unfolding [32,33] has also been found in the structure of thermostable citrate synthase from *Thermoplasma acidophilum* [28].

Tertiary contacts

Perutz and Raidt [34] postulated that the thermostability of clostridial ferredoxins was based on an increased number of salt bridges. In various thermostable proteins a higher number of ion pairs were found, than in their mesostable counterparts [22,35,36]. However, Fd_{Tm} does not seem to be stabilized by an additional number of salt bridges. In fact, only one salt bridge could be found, between Glu38 Oε2 and the amino terminus, which further locks the N terminus to turn D. This salt bridge is also present in Fd_{Daf} (which contains two additional salt

Figure 6

β sheet B1 is fixed to the protein core through main-chain hydrogen bonds. The main-chain atoms from residues Met1 and Val3 of β sheet B1 form hydrogen bonds (grey dotted lines) with main-chain atoms from residues Thr39 and Pro37 of turn D. A similar situation is found in the hyperthermostable Fd_{Pf} [8] and Fd_{Tl} [7].

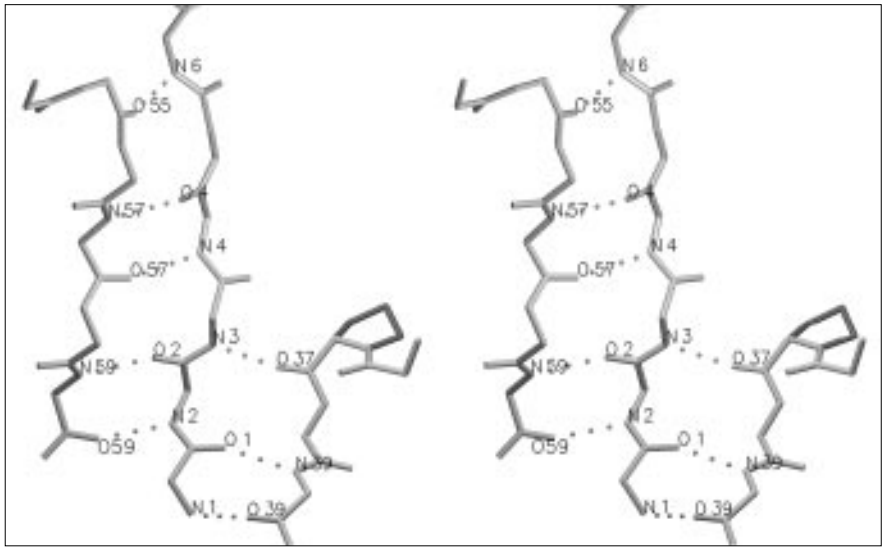

bridges [5]) and in mesophilic dicluster-containing ferredoxins such as Fd_{Pa} [10,11] and Fd_{Av} [37].

More significant, though, seems to be a general increase in the number of hydrogen bonds involving side-chain atoms, which are particularly important in stabilizing the conformations of turns or involved in fixing turns together (Table 4). This difference corresponds to a 50% increase in the total number of side-chain mediated hydrogen bonds for Fd_{Tm} when compared with Fd_{Dg}. Remarkably, 9 out of 14 hydrogen bonds involving side-chain atoms are formed between charged residues and a neutral partner. Table 4 shows a clear correlation between relative thermostability and the number of such hydrogen bonds. Charged-neutral hydrogen bonds have been correlated with the thermostability of several glyceraldehyde-3-phosphate dehydrogenases [38].

Stabilization of turns A and E

Thr53, conserved only in Fd_{Tm} and Fd_{Tl}, is located in turn E, close to the iron-sulfur cluster, just after helix H2. Thr53 Oγ is hydrogen-bonded to Ala9 O (Table 2), forming a bridge between turn E and turn A. In the ferredoxin structure from the moderately thermophile *B. thermoproteolyticus* (Fd_{Bt}) a similar bridging between these turns was observed (Thr63 Oγ and Ser65 Oγ are bonded to Thr10 O [6]). Turn A is additionally stabilized by charged-neutral hydrogen bonds from Lys31 Nζ to Ala7 O and to Cys10 O (Table 2). In Fd_{Daf} and in Fd_{Dg} only one hydrogen bond to the conserved lysine residue is present [4,6].

Bridging between α helix H1 and β strand B2a

The side-chain of Glu17 forms a hydrogen bond to Leu26 N, bridging helix H1 and β strand B2a. In all the other monocluster-type ferredoxins compared in this work, Glu17 is replaced by alanine or valine (Fig. 2). The strength of this particular hydrogen bond (Table 2) and the fact that it is formed between the side chain atom of a charged residue and a main chain atom makes this interaction particularly important for Fd_{Tm}.

Table 4

Comparison of the number of H-bonds in monocluster containing ferredoxins.

Protein	Number of residues	Total H-bonds	Main chain H-bonds	Salt bridges	Side chain H-bonds	Charged-neutral H-bonds
Fd_{Tm}	59	43	29	1	14	9
Fd_{Bt}	81	41	23	1	18	8
Fd_{Dg}	58	34	29	0	7	3
Fd_{Daf} I	64	39	30	3	9	7
Fd_{Daf} II	64	35	28	3	7	4

The values shown in this table were calculated from the tables of putative hydrogen bonds presented in [4–6]. I and II refer to the molecules I and II present in the asymmetric unit of Fd_{Daf}.

Figure 7

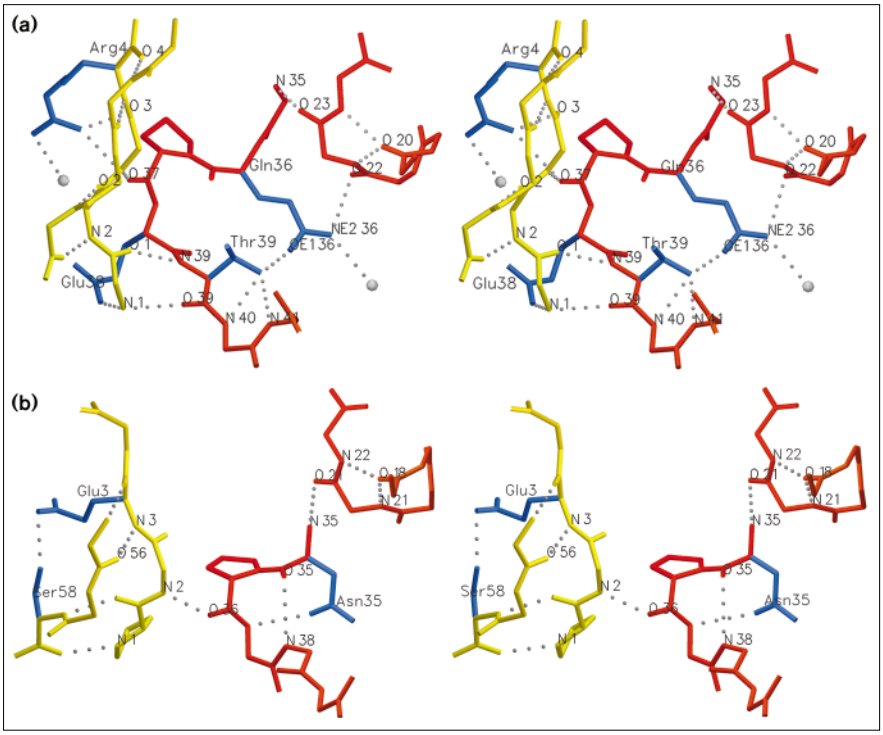

The network of hydrogen bonds connecting the N-terminal β strand (yellow), turn D (red) and turn B (red) is more extensive in Fd_{Tm} (**a**) than in Fd_{Dg} (**b**). The side chains involved in hydrogen bonds are shown in blue and the hydrogen bond network is represented by grey dashed lines. Water molecules are shown as grey spheres. Note: in Fd_{Tm} the N terminus is fixed both by a hydrogen bond to Thr39 and a salt bridge to the side-chain of Glu38.

Hydrogen bond network between β strand B1a, turn B and turn D

The most striking hydrogen bond network is formed between the N-terminal β strand, turn B and turn D (Table 2, Fig. 7a). The side chains of Gln36 and Thr39 are hydrogen-bonded to each other. Hydrogen bonds are further formed from Gln36 Nε2 to Asp22 O and from Leu35 N to Val23 O, tightly fixing turn D to turn B. Turn D is additionally fixed to β strand B1a through strong main-chain to main-chain hydrogen bonds (Fig. 6), through hydrogen bonds formed from Arg4 Nη1 to Pro37 O and also through the salt bridge involving Glu38 (Fig. 7a). In summary, a number of interactions appears to fix the N terminus to turn D, increasing the conformational stability of turn D, and additionally connecting this turn to turn B.

In Fd_{Dg}, residues Asn35–Ser38 form a very stable type I/Asx turn and a hydrogen bond from Ser58 Oγ to Glu3 Oε2 further joins the N-terminal and the C-terminal strands of the first β sheet (Fig. 7); [4]. The polypeptide chain of Fd_{Bt} diverges strongly from the other ferredoxins in this region and can not be included in the comparison. Fd_{Daf} displays a salt bridge between Glu40 and the N terminus, an additional salt bridge is formed between two residues in different strands of β sheet B1 and turn D is also of type I/Asx. Thus, the exposed turn D is generally fixed through tertiary interactions in mesophilic ferredoxins but the total number of stabilizing interactions seems to be increased in Fd_{Tm}.

Concluding remarks

The analysis of the crystallographic structure of Fd_{Tm} reveals a number of stabilizing factors compared with other monocluster-containing ferredoxins from mesophiles. The relevance of the stabilization provided by some of these factors is in certain settings supported by similarities with hyperthermostable Fd_{Tl} and Fd_{Pf} and by similarities with other extremely thermostable proteins. Comparisons with Fd_{Bt} reveal in some cases an intermediate strength in these stabilization factors correlated with the relative thermostability of this ferredoxin. Residues in strained conformations are exchanged with glycines, the alanine content of α helices is increased and turn C (which is located in the most flexible region of the whole protein) is shorter in Fd_{Tm}, Fd_{Tl}, Fd_{Pf} and Fd_{Bt}. Additionally, Fd_{Tm}, Fd_{Tl} and Fd_{Pf} show strong hydrogen bonds fixing the β sheet involving the N and the C terminus to the core of the molecule.

From comparisons between Fd_{Tm} and mesophilic ferredoxins, a general increase in the number of hydrogen bonds is clear. A small number of amino acid exchanges to residues with increased potential to form hydrogen bonds occurs: all these residues (Arg4, Glu17, Gln36, Thr39 and Thr53) except one (Ser57) are involved in forming hydrogen bonds between segments far apart in the sequence or in stabilizing the conformation of turns which constitute potential weak points upon thermal unfolding. Clearly, the contribution of each hydrogen bond to protein stabilization depends on the participating groups and on the location of the

hydrogen bond, not excluding the importance of the bond angle and length. In this context, hydrogen bonding between a charged residue and a neutral partner might contribute favourably to thermostabilization and the number of such hydrogen bonds seems to have a strong correlation with thermostability. All these small, mainly conservative, changes seem to interact cooperatively in order to increase the stability of Fd_{Tm}. The magnitude of the individual effects of these changes on thermostability remains to be measured.

The final result of all these possibly stabilizing features is a more stable polypeptide scaffold which avoids the loss of the relatively exposed iron-sulfur cluster and allows this ferredoxin to exert its redox activity at physiologically high temperatures.

Biological implications

Thermotoga maritima (Tm) has a maximum growth temperature of 90° C Thus, proteins from this hyperthermophilic bacterium are functionally stable at temperatures close to the boiling point of water. A detailed structural comparison between isofunctional proteins from mesophiles and hyperthermophiles is essential for identifying mechanisms of molecular adaptation to extreme temperatures and the identification of structural features that render proteins extremely thermostable is of considerable scientific and biotechnological interest.

Comparison of the high resolution X-ray structures of ferredoxins from the hyperthermophile *Thermotoga maritima* (Fd_{Tm}) with other monocluster-type ferredoxins from mesophiles reveals a number of features that potentially explain the larger thermal stability of Fd_{Tm}. As expected from its high sequence homology, hyperthermostable Fd_{Tm} displays the basic topology of mesostable ferredoxins. However, its α helices are stabilized, its residues in strained conformations are replaced with glycines, its turns are shortened, and it has a general increase in the number of hydrogen bonds. In particular, hydrogen bonds from charged residues to main-chain atoms or uncharged side chains are increased. The local structure in the region where each of these hydrogen bonds is formed has to be analyzed to understand the relative importance of different hydrogen bonds to thermostabilization. In Fd_{Tm}, hydrogen bonds specifically stabilize turns or fix turns and other secondary structure elements.

The role of particular interactions, which have been revealed by the crystal structure of Fd_{Tm}, on its high thermostability may now be evaluated via site-directed mutagenesis accompanied by structural studies of the mutants.

High resolution X-ray structures of proteins from a variety of hyperthermophiles have suggested that factors such as increased numbers of salt bridges, decrease in the accessible surface area, or burying of hydrophobic residues, influence thermal stability. However, no differences are found between Fd_{Tm} and mesostable ferredoxins with respect to these features. Clearly, different proteins use distinct dominating forces for maintaining their stability and functional integrity at extreme temperatures.

Materials and methods

Crystallization

Fd_{Tm} was expressed heterologously in *E. coli* and purified as described by Darimont and Sterner [3]. The initial screening for the crystallization conditions of Fd_{Tm} was done with Crystal Screen and Crystal Screen II sparse matrix crystallization kits (Hampton Research). The best crystals were obtained using the hanging drop vapour diffusion method from drops containing 5 μl of protein solution (8 mg ml^{-1} in water) and 10 μl of 3.2 M ammonium sulfate, 0.1 M TRIS-Cl pH 7.5, equilibrated against 1 ml of the latter solution at 20° C.

Elongated prisms grew within one week belonging to the space group $P2_12_12_1$ with cell constants a = 29.63 Å, b = 38.02 Å, c = 44.36 Å. The size of the unit cell indicated the presence of one ferredoxin molecule per asymmetric unit and a solvent content of 33 %.

X-ray data collection

Diffraction data up to 1.7 Å resolution were collected on a MARresearch imaging plate attached to a Rigaku rotating anode generator RU200 providing CuK_α radiation. Data were evaluated with the MOSFLMv5.23 package [39] and scaling, merging and reduction of the integrated intensities was performed with the CCP4 package [40] . Details of the data collection parameters and statistics are depicted in Table 5.

Patterson search

Desulfovibrio gigas 1[3Fe–4S] ferredoxin II (Fd_{Dg}) [4] was used as a search model. This protein shares a 43 % identity with *T. maritima* ferredoxin and the whole protein without any alteration of amino acids was used for the Patterson search [41]. Data in the resolution range 10–4 Å were used in both rotation and translation functions computed with AMoRe [42]. Using a Patterson cut-off radius of 19.7 Å, 1000 rotation function peaks were obtained with the top peak having an AMoRe correlation coefficient (CC) of 16.8 %. The next highest peak in the rotation function showed a CC of 12.5 %. Using the top peak of the previous rotation function, the translation function gave a top solution with a CC of 44.5 % (with a R value of 43.3 %). The next highest solution for the translation function had a CC of 30.8 %. This model was then subjected to rigid-body refinement (fiting) within AMoRe to give a CC of 47.1 % with an initial R factor of 41.9 %, while the next highest peak showed a CC of 27.5 %.

Refinement

Rigid-body refinement of the rotated and translated Fd_{Dg} model by means of XPLOR [43], was performed to further refine its orientation and position, using data between 10 and 2.5 Å resolution. The model used for this refinement was altered so that the non-conserved residues were mutated to alanines, the last two C-terminal residues were removed and additionally the conserved phenylalanine was replaced with alanine to check the correctness of the solution from AMoRe. The R factor at this stage was 45.8 %. Further energy restrained positional refinement, using the parameters derived by Engh and Huber [44], decreased the R factor to 39.2 %. An initial $2F_o–F_c$ map at 2.0 Å was calculated and the density showed clearly the presence of the phenylalanine side-chain as well as other large side chains such as Glu16. The additional iron present in the cluster of Fd_{Tm} was already visible in the density as was the different orientation of the cysteine sulfhydryl group that binds this iron. The complete fitting of Fd_{Tm} sequence to the observed density was achieved through successive

cycles of manual building with O [45] on sequentially overlapping $3F_o–2F_c$ omit maps and crystallographic refinement with X-PLOR. The resolution was progressively increased in steps of 0.2 Å until a maximum value of 1.75 Å. During the initial steps of refinement the target values used for the stereochemical restraint of the [4Fe–4S] complex were based on the values reported by Merrit *et al.* [37]; additionally, the force constants for all distance and angle constraints in the cluster were set to 500 and 2000 kJ mol^{-1}, respectively, to avoid distortion of the cluster. Refinement of individual B values started at 31.0 % R factor. Water molecules were added at stereochemically reasonable positions of high difference density using the molecular graphics program MAIN [46]. At this stage the force field constants for the angle constraints were decreased to 300 kJ mol^{-1} for the distances and to 20 kJ mol^{-1} for the angles. Finally individual anisotropic B factor refinement of the data performed with X-PLOR improved the map and particularly the residual density observed around the [4Fe–4S] cluster. The final crystallographic R value for the reflections between 10 and 1.75 Å resolution is 15.9 % (Table 5).

Final model

The final model comprises 59 amino acid residues, one [4Fe–4S] cluster and 40 water molecules.

The complete polypeptide chain could be traced with exception of the C-terminal Glu60. The last side-chain atoms from residues Lys2, Asp40, Lys45 and Glu59 were not clearly visible in the density and could not be adequately modeled.

The quality of the final refined structure was assessed with PROCHECK [47]. A Ramachandran plot for Fd_{Tm} shows that 91.7 % of the residues lie in the most favoured regions. The residues Cys20, Val23, Gln36 and Thr53 are located in additionally allowed regions. No residues in generously allowed or even in disallowed regions were observed.

The distribution of the mean temperature factors indicates that the region comprising residues Gly27 to Gly30 has the highest B values, followed by the C terminus which is not well defined in the density. Residues exposed in the outer part of the molecule such as Asp8, Glu38 and Asp40 also show relatively high temperature factors.

Structure comparison

The comparison and superposition of the ferredoxin structures was made with LSQMAN [48]. Figure 2 was made with ALSCRIPT [49]. Figures 1,3–7 were made with SETOR [50].

Table 5

Summary of data collection and processing statistics.

Resolution range (Å)	19.2–1.7
Number of measured reflections	36 264
Number of unique reflections	5864
Average multiplicity	5.4
R_{merge}* (%)	7.8
Completeness (overall) (%)	97.9
Completeness (1.81–1.75 Å) (%)	93.1
Number of protein atoms	428
Number of water molecules	40
Rmsd distances	0.009
Rmsd bond angles	1.856
R-factor (10–1.75 Å) (%)	15.9
Average B factor for protein atoms (Å^2)	19.4
Average B factor for water molecules (Å^2)	36.4

*$R_{merge} = \Sigma(\Sigma|I(h)i - <I(h)>|/\Sigma<I(h)>)$; $I(h)i$ is the observed intensity of the i-th measurement of reflection h, and $<I(h)>$ the mean intensity of the reflection; calculated after scaling and merging with CCP4 [40].

Accession numbers

The coordinates have been deposited in the Brookhaven Protein Databank (code 1VJW).

Acknowledgements

The participants and organizers of the CSHL course in 'Macromolecular Crystallography' (1994) are greatly acknowledged for the enthusiastic support and helpful suggestions during the initial stages of this project. We thank Andrea Löschmann for excellent technical assistance and Prof Kasper Kirschner for continuous support. Thanks, too, to FX Gomis-Rüth, R Engh, M Stubbs and A Messerschmidt for helpful discussions. This work was supported by grant PraxisXXI/BD/4050/94 from Junta Nacional de Investigação Ciêntifica e Tecnológica (JNICT) to S Macedo-Ribeiro and by a grant of the Swiss National Science foundation (31-32369.91) to Prof K Kirschner.

References

1. Beinert, H. (1990). Recent developments in the field of iron-sulfur proteins. *FASEB J.* 4, 2483–2491.
2. Blamey, J.M., Mukund, S. & Adams, M.W. (1994). Properties of a thermostable 4Fe-ferredoxin from the hyperthermophilic bacterium *Thermotoga maritima*. *FEMS Microbiol. Lett.* 121, 165–169.
3. Darimont, B. & Sterner, R. (1994). Sequence, assembly and evolution of a primordial ferredoxin from *Thermotoga maritima*. *EMBO J.* 13, 1772–1781.
4. Kissinger, C., Sieker, L., Adman, E. & Jensen, L. (1991). Refined crystal structure of ferredoxin II from *Desulfovibrio gigas* at 1.7 Å. *J. Mol. Biol.* 219, 693–715.
5. Séry, A., *et al.*, & Roth, M. (1994). Crystal structure of the ferredoxin from *Desulfovibrio africanus* at 2.3 Å resolution. *Biochemistry* 33, 15408–15417.
6. Fukuyama, K., Matsubara, H., Tsukihara, T. & Katsube, Y. (1989). Structure of [4Fe-4S] ferredoxin from *Bacillus thermoproteolyticus* at 2.3 Å resolution. *J. Mol. Biol.* 210, 383–398.
7. Donaire, A., Zhou, Z., Adams, M.W.W. & La Mar, G.N. (1996). ^{1}H NMR investigation of the secondary structure, tertiary contacts and cluster environment of the four-iron ferredoxin from the hyperthermophilic Archaeon *Thermococcus litoralis*. *J. Biomol. NMR* 7, 35–47.
8. Teng, Q., *et al.*, & La Mar, G.N.(1994). Solution ^{1}H NMR determination of secondary structure for the three-iron form of ferredoxin from the hyperthermophilic Archaeon *Pyrococcus furiosus*. *Biochemistry* 33, 6316–6326.
9. Sticht, H., *et al.*, & Rösch, P. (1996). An NMR-derived model for the solution structure of oxidized *Thermotoga maritima* 1[Fe4–S4] ferredoxin. *Eur. J. Biochem.* 55, 1–10.
10. Adman, E.T., Sieker, L.C. & Jensen, L.H. (1973). Structure of a bacterial ferredoxin. *J. Biol. Chem.* 248, 3987–3996.
11. Adman, E.T., Sieker, L.C. & Jensen, L.H. (1976). Structure of *Peptococcus aerogenes* ferredoxin. *J. Biol. Chem.* 251, 3801–3806.
12. Stout, C.D. (1993). Crystal structures of oxidized and reduced *Azobacter vinelandii* ferredoxin at pH 8 and 6. *J. Biol. Chem.* 268, 25920–25927.
13. Duée, E.D., *et al.*, & Moulis, J.M. (1994). Refined crystal structure of the 2[4Fe–4S] ferredoxin from *Clostridium acidiuruci* at 1.84 Å resolution. *J. Mol. Biol.* 243, 683–695.
14. Rees, D.C., Lewis, M. & Lipscomb, W.N. (1983). Refined crystal structure of carboxy peptidase A at 1.54 Å resolution. *J. Mol. Biol.* 168, 367–387.
15. Gorst, C.M., *et al.*, & La Mar, G.N. (1995). Participation of the disulfide bridge in the redox cycle of the ferredoxin from the hyperthermophile *Pyrococcus furiosus*: ^{1}H nuclear magnetic resonance time resolution of the four redox states at ambient temperature. *Biochemistry* 34, 8788–8795.
16. Macedo, A.l., *et al.*, & Moura, J.J. (1994). Thiol/disulfide formation associated with the redox activity of the [3Fe–4S] cluster of *Desulfovibrio gigas* ferredoxin II. ^{1}H NMR and Mössbauer spectroscopic study. *J. Biol. Chem.* 269, 8052–8058.
17. Backes, G., *et al.*, & Sandres-Loehr, J. (1991). The environment of Fe_4S_4 clusters in ferredoxins and high-potential iron proteins. New information from X-ray crystallography and resonance Raman spectroscopy. *J. Am. Chem. Soc.* 113, 2055–2064.
18. Jensen, G.M., Warshel, A. & Stephens, P.J. (1994). Calculation of the redox potentials of iron-sulfur proteins: the 2-/3- couple of $[Fe_4S_4Cys_4]$ clusters in *Peptococcus aerogenes* ferredoxin, *Azobacter vinelandii* ferredoxin I, and in *Chromatium vinisum* high-potential iron protein. *Biochemistry* 33, 10911–10924.

19. Smith, E.T., Blamey, J.M., Zhou, Z.H. & Adams, M.W.W. (1995). A variable-temperature direct electrochemical study of metalloproteins from hyperthermophilic microorganisms involved in hydrogen production from pyruvate. *Biochemistry* **34**, 7161–7169.
20. Hatchikian, E.C., *et al.*, Thomson, A.J. (1984). Spectroscopic characterization of ferredoxin I and II from *Desulfovibrio africanus*. *Biochem. Biophys. Acta* **784**, 40–47.
21. Cammack, R., *et al.*, & Gayda, J.P. (1977). Spectroscopic studies of the oxidation-reduction properties of three forms of ferredoxin from *Desulfovibrio gigas*. *Biochem. Biophys. Acta* **490**, 311–321.
28. Hennig, M., Darimont, B., Sterner, R., Kirschner, K. & Jansonius, J.N. (1995). 2.0 Å structure of indole-3-glycerol phosphate synthase from the hyperthermophile *Sulfolobus solfataricus*: possible determinants of protein stability. *Structure* **3**, 1295–1306.
22. Wildegger, G., *et al.*, & Rösch, P. (1995). ^{1}H nuclear magnetic resonance investigation of oxidized ferredoxin from *Thermotoga maritima*. *Eur. J. Biochem.* **229**, 658–668.
23. Devanathan, T., Akagi, J.M., Hersh, R.T. & Himes, R.H. (1969). Ferredoxins from two thermophilic *Clostridia*. *J. Biol. Chem.* **11**, 2846–2853.
24. Yang, S.-S., Ljungdahl, L.G. & LeGall, J. (1977). A four-iron, four-sulfide ferredoxin with high thermostability from *Clostridium thermoaceticum*. *J. Bacteriol*. **130**, 1084–1090.
25. Menendez-Arias, L. & Argos, P. (1989). Engineering protein thermal stability. Sequence statistics point to residue substitutions in α helices. *J. Mol. Biol.* **206**, 397–406.
26. Kelly, C.A., Nishiyama, M., Ohnishi, Y., Beppu, T. & Birktoft, J.J. (1993). Determinants of protein thermostability observed in the 1.9 Å crystal structure of malate dehydrogenase from the thermophilic bacterium *Thermus flavus*. *Biochemistry* **32**, 3913–3922.
27. Russell, R.J.M., Hough, D.W., Danson, M.J. & Taylor, G.L. (1994). The crystal structure of citrate synthase from the thermophilic archaeon, *Thermoplasma acidophilum*. *Structure* **2**, 1157–1167.
29. Ishikawa, K., Kimura, S., Kanaya, S., Morikawa, K. & Nakamura, H. (1993). Structural studies of mutants of *Escherichia coli* ribonuclease H1 with enhanced thermostability. *Protein Eng.* **6**, 85–91.
30. von der Osten, C., *et al.*, & Mikkelsen, J.M. (1993). Protein engineering of subtilisins to improve stability in detergent formulations. *J. Biotechnol.* **28**, 55–58.
31. Day, M.W., *et al.*, & Rees, D.C. (1992). X-ray crystal structures of the oxidized and reduced forms of the rubredoxin from the marine hyperthermophilic archaebacterium *Pyrococcus furiosus*. *Protein Sci.* **1**, 1494–1507.
32. Zhou, H.X., Hoess, R.H. & DeGrado, W.F. (1996). *In vitro* evolution of thermodynamically stable turns. *Nat. Struct. Biol.* **3**, 446–451.
33. Daggett, V. & Levitt, M. (1993). Protein unfolding pathways explored through molecular dynamic simulations. *J. Mol. Biol.* **232**, 600–619.
34. Perutz, M.F. & Raidt, H. (1975). Stereochemical basis of heat stability in bacterial ferredoxins and in haemoglobin A2. *Nature* **255**, 256–259.
35. Korndörfer, I., Steipe, B., Huber, R., Tomschy, A. & Jaenicke, R. (1995). The crystal structure of holo-glyceraldehyde-3-phosphate dehydrogenase from the hyperthermophilic bacterium *Thermotoga maritima* at 2.5 Å resolution. *J. Mol. Biol.* **246**, 511–521.
36. Yip, K.S.P., *et al.*, & Rice, D.W. (1995). The structure of *Pyrococcus furiosus* glutamate dehydrogenase reveals a key role for ion-pair networks in maintaining enzyme stability at extreme temperatures. *Structure* **3**, 1147–1158.
37. Merrit, E., Stout, G., Turley, S., Sieker, L. & Jensen, L. (1993). Structure at pH 6.5 of ferredoxin I from *Azobacter vinelandii* at 2.3 Å resolution. *Acta Cryst. D* **49**, 272–281.
38. Tanner, J.J., Hecht, R.M. & Krause, K.L. (1996). Determinants of enzyme thermostability observed in the molecular structure of *Thermus aquaticus* D-glyceraldehyde-3-phosphate dehydrogenase at 2.5 Å resolution. *Biochemistry* **35**, 2597–2609.
39. Leslie, A. (1991). Macromolecular Data Processing. In *Crystal. Computing V*. (Moras, D., Podjarny, A.D. & Thierry, J.C., eds), pp. 27–38, Oxford University Press, Oxford, UK.
40. Collaborative Computational Project No. 4. (1994). The CCP4 suite: programs for protein crystallography. *Acta Cryst. D* **50**, 760–763.
41. Huber, R. (1965). Die Automatisierte Faltmolekülmethode. *Acta Cryst. A* **19**, 353–356.
42. Navaza, J. (1994). An automated package for molecular replacement. *Acta Cryst. A* **50**, 157–163.
43. Brünger, A., Kuryian, K. & Karplus, M. (1987). Crystallographic R factor refinement by molecular dynamics. *Science* **235**, 458–460.
44. Engh, R. & Huber, R. (1991). Accurate bond and angle parameters from X-ray protein structure refinement. *Acta Cryst. A* **47**, 392–400.
45. Jones, T., Zou, J., Cowan, S. & Kjeldgaard, M. (1991). Improved methods for building protein models in electron density maps and the location of errors in these models. *Acta Cryst. A* **47**, 110–119.
46. Turk, D. (1992). Weiterentwicklung eines Programms für Molekülgraphik und Elektronendichte-Manipulation und seine Anwendung auf verschiedene Protein-Stukturaufklärungen. Ph.D. thesis. Technische Universität, München.
47. Laskowski, R., MacArthur, M., Hutchinson, E. & Thorton, J. (1993). PROCHECK: a program to check the stereochemical quality of protein structures. *J. Appl. Cryst.* **26**, 283–291.
48. Kleywegt, G.J. & Jones, T.A. (1994). A super position. *ESF/CCP4 Newsletter* **31**, 9–14.
49. Barton, G.J. (1993). ALSCRIPT. A tool to format multiple sequence alignments. *Protein Eng.* **6**, 37–40.
50. Evans, S.V. (1990). SETOR: hardware lighted three-dimensional solid model representations of macromolecules. *J. Mol. Graphics* **11**, 134–138.
51. Busse, S.C., *et al.*, & Adams, M.W. (1992). Proton NMR investigation of the oxidized three-iron clusters in the ferredoxins from the hyperthermophilic archaea *Pyrococcus furiosus* and *Thermococcus litoralis*. *Biochemistry* **31**, 11952–11962.
52. Bruschi, M. (1979). Amino acid sequence from *Desulfovibrio gigas*: revisions. *Biochem. Biophs. Res. Commun.* **91**, 623–628.
53. Fukuyama, K., Nagahara, Y., Tsukihara, T. & Katsube, Y. (1988). Tertiary structure of *Bacillus Thermoproteolyticus* [4Fe–4S] ferredoxin: evolutionary implications for bacterial ferredoxins. *J. Mol. Biol.* **199**, 183–193.
54. Davy, S.L., *et al*., & Moore, G.R. (1994). MCD and 1H NMR spectroscopic studies of Desulfovibrio africanus ferredoxin I: revised amino acid sequence and identification of secondary structure. *Biochem. Biophys. Acta.* **1209**, 33–39.